

# Straightforward Solvothermal Synthesis toward Phase Pure $\text{Li}_2\text{CoPO}_4\text{F}$

Jürgen Schoiber,<sup>\*,†</sup> Raphael J. F. Berger,<sup>†</sup> Johannes Bernardi,<sup>‡</sup> Mario Schubert,<sup>§</sup> Chihiro Yada,<sup>||</sup> Hidenori Miki,<sup>||</sup> and Nicola Hüsing<sup>\*,†</sup>

<sup>†</sup>Institute of Materials Chemistry, Paris-Lodron University Salzburg, Hellbrunnerstraße 34, Salzburg, 5020, Austria

<sup>‡</sup>Vienna University of Technology, Wiedener Hauptstraße 8-10/052, Wien, 1040, Austria

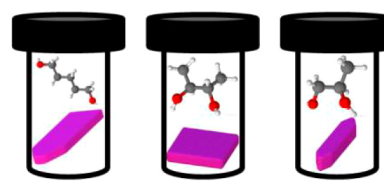
<sup>§</sup>Institute of Molecular Biology, Paris-Lodron University, Billrothstraße 11, Salzburg, 5020, Austria

<sup>||</sup>Battery Research Division, Toyota Motor Corporation Higashifuji Technical Center, 1200 Mishuku, Susono, Shizuoka 410-1193, Japan

## S Supporting Information

**ABSTRACT:**  $\text{Li}_2\text{CoPO}_4\text{F}$ , a promising high potential cathode material, has been synthesized for the first time via a one-pot solvothermal synthesis route. The characterization with respect to its crystal structure and electrochemical performance in a lithium half-cell is reported. Scanning electron microscopy, transmission electron microscopy, and X-ray diffraction studies reveal a strong influence of the solvent on the purity of the obtained crystalline phases and the particle morphology with preferred crystal growth orientations. The electrochemical tests of carbon coated materials demonstrate excellent characteristics in terms of high capacity.

## Solvothermally prepared $\text{Li}_2\text{CoPO}_4\text{F}$



## INTRODUCTION

Alkali transition metal fluoride phosphate compounds with the formula  $\text{A}_{2-x}\text{T}^{2+x}\text{PO}_4\text{F}$  ( $\text{A} = \text{Na}, \text{Li}$ ;  $\text{T} = \text{Ti}, \text{V}, \text{Mn}, \text{Fe}, \text{Co}, \text{Ni}$ ) are under investigation as possible electrode materials for next generation alkali-ion battery systems.<sup>1–8</sup> Despite their common stoichiometric composition, different types of crystal structures are found for these compounds. For instance  $\text{Na}_2\text{TPO}_4\text{F}$  ( $\text{T} = \text{Fe}, \text{Co}$ ) crystallizes in the space group  $Pbcn$ , while the lithium-homologues such as  $\text{Li}_2\text{CoPO}_4\text{F}$ ,  $\text{Li}_2\text{NiPO}_4\text{F}$ , and  $\text{Li}_2\text{FePO}_4\text{F}$  crystallize in the space group  $Pnma$ . Furthermore,  $\text{Li}_2\text{FePO}_4\text{F}$  shows a polymorphic behavior with structures in the space groups  $Pbcn$  or  $P\bar{1}$  depending on the synthesis conditions employed.<sup>1,2,7,9–11</sup>

As battery materials,  $\text{Li}_2\text{TPO}_4\text{F}$  type compounds provide higher voltages and higher capacities compared to the Na-analogues and therefore lead to higher energy densities in devices.<sup>3,9</sup> With an operating voltage of around 5 V and a theoretical capacity of 287 mAh  $\text{g}^{-1}$   $\text{Li}_2\text{CoPO}_4\text{F}$  got into the focus of recent research activities.<sup>12</sup> The structure (space group  $Pnma$ ) is composed of infinite chains of  $\text{CoO}_4\text{F}_2$  octahedra with the fluorine atoms occupying axial or equatorial trans configurations depending on the respective crystallographic position of the Co-atom (Figure 1).<sup>1,11</sup> The phosphate tetrahedra link chains of  $\text{CoO}_4\text{F}_2$  octahedra via common vertices and offer three different Li-positions (Li(1), Li(2), Li(3)) in the 3D-framework. First DFT-based calculations suggested three-dimensional (3D) diffusion pathways for the Li-ions,<sup>13</sup> however, more recent investigations only support the

hypothesis of a one-dimensional (1D) pathway for only the Li-ion (Li(1)).<sup>14</sup> This result is in agreement with the finding that a successful extraction of more than one Li-ion per formula unit could not be achieved so far.<sup>12,15</sup> In addition, a poor cycling performance was observed probably due to the high operating voltage.<sup>15–17</sup> This could be overcome by protective coating measures, i.e., using  $\text{Li}_3\text{PO}_4$  or  $\text{ZrO}_2$ , to suppress etching of the cathode material and formation of decomposition products during electrochemical cycling.<sup>12,18</sup> Besides coating of  $\text{Li}_2\text{CoPO}_4\text{F}$ , the addition of  $\text{SiO}_2$  nanoparticles to the active material or the use of fluorinated electrolytes gave similar results.<sup>14,19</sup> Recently, a full cell setup consisting of  $\text{Li}_2\text{CoPO}_4\text{F}$  as cathode material and  $\text{Li}_3\text{PO}_4$ -coated  $\text{TiO}_2$  anatase nanotubes as anode material showed remarkable discharge capacities (130 mAh  $\text{g}^{-1}$ ) after 240 cycles with an operating voltage of 3 V, proving that  $\text{Li}_2\text{CoPO}_4\text{F}$  can be considered in high energy density lithium ion batteries.<sup>20</sup>

So far only solid state reaction-based synthesis routes with rather narrow synthesis condition windows, have been reported for the preparation of  $\text{Li}_2\text{CoPO}_4\text{F}$ .<sup>15,16,21,22</sup>  $\text{Li}_2\text{CoPO}_4\text{F}$  appears to be metastable at temperatures above 700 °C, where a decomposition into  $\text{Li}_3\text{PO}_4$  and  $\text{LiCoPO}_4$  occurs.<sup>15</sup> But not only the reaction temperature is a crucial synthesis parameter, also the reaction time as well as subsequent quenching show a

Received: April 14, 2016

Revised: July 20, 2016

Published: August 1, 2016

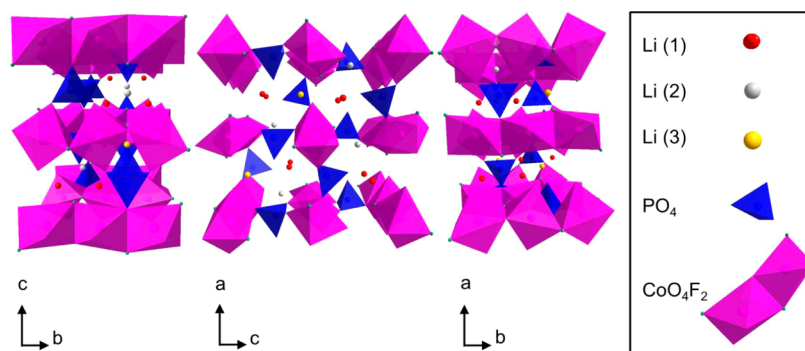


**Figure 1.** Crystal structure of  $\text{Li}_2\text{CoPO}_4\text{F}$  visualized along different projections. The three different Li-ion positions are represented by differently colored spheres. The  $\text{PO}_4$ -tetrahedra and the  $\text{CoO}_4\text{F}_2$  octahedra are shown in blue and pink, respectively, including the  $\text{F}^-$ -ions as small green spheres.

significant influence on the purity and electrochemical performance of the synthesized  $\text{Li}_2\text{CoPO}_4\text{F}$ .<sup>16,21,22</sup> Longer reaction times or naturally cooling to room temperature lead to decomposition products, such as  $\text{LiCoPO}_4$  and  $\text{Li}_3\text{PO}_4$ .<sup>16,22</sup> Also lower capacities were achieved from  $\text{Li}_2\text{CoPO}_4\text{F}$  materials synthesized at higher reaction temperatures due to the occurrence of decomposition byproducts.<sup>16</sup> However, in  $\text{Na}_2\text{CoPO}_4\text{F}$  no such dependence of product composition on reaction temperature or cooling procedure is observed and subsequent quenching to room temperature is not necessary.<sup>6</sup> The same has been found for  $\text{Na}_2\text{FePO}_4\text{F}$  and  $\text{Na}_2\text{MnPO}_4\text{F}$ .<sup>7,23</sup>

Apart from the developed solid state reactions and sol-gel synthesis routes for the above mentioned compounds, wet chemistry synthesis routes were used for different Li- and Na-based transition metal fluoride phosphate cathode materials, applying hydrothermal, solvothermal as well as ionothermal conditions, for the synthesis of, e.g.,  $\text{Li}_2\text{FePO}_4\text{F}$ ,  $\text{Na}_2\text{FePO}_4\text{F}$ , or  $\text{Na}_2\text{MnPO}_4\text{F}$ .<sup>24–27</sup> So far no wet chemistry synthesis method for  $\text{Li}_2\text{CoPO}_4\text{F}$  has been reported.

Recently, we developed a simplified synthesis protocol to obtain  $\text{Li}_2\text{CoPO}_4\text{F}$  by a two step approach.<sup>28</sup> A solvothermally prepared  $\text{LiCoPO}_4/\text{LiF}$  powder could be converted into  $\text{Li}_2\text{CoPO}_4\text{F}$  at 660 °C within an hour reaction time. The obtained compounds were investigated regarding their electrochemical properties. On the basis of our previous results we herein report a new and simple one-pot solvothermal approach for the synthesis of phase pure  $\text{Li}_2\text{CoPO}_4\text{F}$ . The crystalline nature and phase composition of the material is strongly influenced by the solvent properties as well as the reaction parameters, e.g., time, which will be discussed in detail. The obtained materials are carbon coated and the influence of the coating procedure on the particle morphology is also investigated.  $\text{Li}_2\text{CoPO}_4\text{F}$  from solvothermal synthesis approaches shows a remarkable electrochemical behavior with a capacity reaching the theoretical capacity of 143 mAh  $\text{g}^{-1}$  indicating that one lithium ion per formula unit is extracted.

## EXPERIMENTAL SECTION

**Material Synthesis.** LiOH, LiCl, and ethylene glycol (99.5%) were purchased from Sigma-Aldrich.  $\text{Co}(\text{OH})_2$  and  $\text{NH}_4\text{F}$  were purchased from Alfa Aesar. Phosphoric acid (85 wt % solution), diethylene glycol (99%), glycerol (99%), tetraethylene glycol (98%), tetraethylene glycol dimethyl ether (98%), 1,5-pentane diol (97%), 2,3-butane diol (98%) from Merck. PEG-400 (99%) was from Roth, 1,2-propane diol from Alfa Aesar, and  $\text{LiPF}_6$  (99.8%), fluoroethylene carbonate (99.5%) and dimethyl carbonate (98%) were purchased

from KISHIDA CHEMICAL Co., Ltd. All chemicals were used without further purification.

The synthesis was conducted as follows: 130 g of the solvent were given into the Teflon-inlet of a stainless steel autoclave with a maximum volume of 200 mL. Upon heating the solvent to 90 °C, the other reagents were added in the following order under constant stirring:  $\text{H}_3\text{PO}_4$  (2.3 g, 85 wt %, 0.02 mmol), LiOH (0.48 g, 0.02 mmol),  $\text{Co}(\text{OH})_2$  (1.86 g, 0.02 mmol), LiCl (1.7 g, 0.04 mmol) and  $\text{NH}_4\text{F}$  (0.74 g, 0.02 mmol). After sealing the autoclave, the suspension was heated to 215 °C within 1 h and kept there for 24 or 36 h. The reaction mixture was then allowed to cool to room temperature. A blue or pink precipitate in almost quantitative yield was collected, centrifuged and washed one time with a mixture of 100 mL of ethanol/deionized water (1:1 v./v.) and one time with 100 mL deionized water with intermediate centrifugation at 4000 rpm for 3 min. The wet powders were dried at 90 °C for 1 h.

**Carbon Coating.** The obtained powders were mixed with 15 wt % vapor grown carbon fibers (VGCF) and ball milled in zirconia crucibles at 300 rpm for 20 h in a Pulverisette 7 (Fritsch). The obtained mixture was annealed at 500 or 600 °C for 1 h (heating rate of 5 °C  $\text{min}^{-1}$ ) under steady argon flow and after cooling to room temperature, the powder has been dried at 120 °C in vacuum for 10 h.

**X-ray Diffraction.** Powder X-ray diffraction (PXRD) measurements ( $5^\circ \leq 2\theta \leq 80^\circ$ , continuous scan) were carried out in reflection-mode on a BRUKER D8 DaVinci Design diffractometer using  $\text{CuK}\alpha$  radiation, fixed  $0.3^\circ$  divergence slit, primary and secondary slit 0.04 rad Soller slits, antiscatter slit  $4.0^\circ$  and a Lynxeye detector (opening angle  $2.93^\circ$ ). Rietveld Refinement: The data refinement was done using the FULLPROF-suite of programs.<sup>29</sup> The pseudo-Voigt function was chosen to model peak shape, all atoms were refined using isotropic atomic displacement parameters. Starting values for the refinement of PXRD data were taken from the literature.<sup>11</sup> To determine the crystallinity of as-synthesized and carbon coated  $\text{Li}_2\text{CoPO}_4\text{F}$  compounds, diamond powder was taken as 100 % crystalline internal standard for PXRD. The mass fractions of  $\text{Li}_2\text{CoPO}_4\text{F}$  and diamond were determined by Rietveld refinement and the crystallinity was calculated by the following equation according to ref 30

$$\text{crystallinity} = \frac{m\%_{\text{crystalline Li}_2\text{CoPO}_4\text{F}}}{m\%_{\text{diamond}}} \cdot \frac{m[\text{mg}]_{\text{diamond}}}{m[\text{mg}]_{\text{Li}_2\text{CoPO}_4\text{F}}}$$

Elemental analysis was conducted at a Vario Micro Cube (Elementar, Germany) to determine the carbon content by combustion.

$^1\text{H}$ - and  $^{13}\text{C}$ -NMR spectra were recorded on a Bruker AVANCE III HD Spectrometer (600 MHz) in  $\text{DMSO}-d_6$ .

$\text{N}_2$ -sorption measurements were carried out on an ASAP2420 (Micromeritics, USA) at  $-196^\circ\text{C}$ . The samples were degassed at 100 °C for 3 h prior to the measurements. The specific surface areas were determined by the BET method in a relative pressure range  $p/p_0$  from 0.05–0.3.<sup>31</sup>

Scanning Electron Microscopy (SEM) images were taken using a ZEISS FE-SEM ULTRAPLUS (ZEISS, Germany) with an in-lens secondary electron detector at an accelerating voltage of 5 kV.

**Transmission Electron Microscopy.** The microstructure of the samples was studied by transmission electron microscopy (TEM) with a TECNAI F20 field emission electron microscope operated at an accelerating voltage of 200 kV. Images were recorded with a Gatan Orius SC600 CCD camera. Structural properties were investigated by selected area electron diffraction or from diffractograms from high resolution lattice fringe images. Electron diffraction patterns were analyzed using the JEMS software package.

**Electrochemical Measurements.** The electrochemical performance of carbon coated  $\text{Li}_2\text{CoPO}_4\text{F}$  particles ( $\text{Li}_2\text{CoPO}_4\text{F}/\text{C}$ ) as an active cathode material was tested in coin-type Li cells (rechargeable battery type CR) assembled in an argon-filled glovebox. For the cell preparation a slurry by using *N*-methylpyrrolidone as solvent and a mixture of  $\text{Li}_2\text{CoPO}_4\text{F}/\text{C}$ , acetylene black (AB) and polyvinylidene difluoride with a weight ratio of 90:5:5 (300 mg:16.7 mg: 16.7 mg) was coated on an aluminum foil as current collector and dried at 120 °C under vacuum. As non-aqueous electrolyte a 1 M solution of  $\text{LiPF}_6$  in a mixture of fluoroethylene carbonate and dimethyl carbonate (1:4 v./v.) was taken. The galvanostatic cycling tests of the cells were performed between 3.0 and 5.3 V with lithium foil as anode at various C-rates (1.0 C = 143 mAh  $\text{g}^{-1}$ ) on a VPM 3 (MultiPotentiostat/Galvanostat/EIS) from Bio-Logic Science Instruments.

## RESULTS AND DISCUSSION

**Solvothermal Synthesis of  $\text{Li}_2\text{CoPO}_4\text{F}$ .** The synthesis of other promising cathode materials for lithium ion batteries, e.g.,  $\text{LiMPO}_4$  ( $M = \text{Fe}, \text{Mn}, \text{Co}$ ),  $\text{Li}_2\text{MnSiO}_4$ ,  $\text{LiFeSO}_4\text{F}$ , or  $\text{LiFePO}_4\text{F}$ , via solvothermal approaches using different solvents, such as monoethylene, tetraethylene or polyethylene glycol at various temperatures ranging from 150 to 400 °C, has previously been reported.<sup>4,32–36</sup> These results and our own newly developed two step synthesis for  $\text{Li}_2\text{CoPO}_4\text{F}$  prompted us to investigate a variety of synthesis parameters with the aim to develop a solvothermal strategy toward  $\text{Li}_2\text{CoPO}_4\text{F}$ .<sup>28</sup>

In our experiments, we first tested the influence of a variety of solvents on the formation of  $\text{Li}_2\text{CoPO}_4\text{F}$ . The focus was on different diol- and ether-based organic solvents, for which the abbreviations and physical properties are listed in Table 1.<sup>37</sup>

**Table 1.** Used Solvents Related Boiling Points [°C], Polarities [ $E_T(30)$ ], and Abbreviation [Number]

solvent	boiling point [°C]	solvent polarity $E_T(30)$ [kcal $\text{mol}^{-1}$ ]	abbreviation [number]
monoethylene glycol	199	56.3	1
glycerol	290	57.0	2
diethylene glycol	244	53.8	3
tetraethylene glycol	314	52.2	4
tetraethylene glycol dimethyl ether	275	39.3 (calc.)	5
PEG-400	>200	51.8 (calc.)	6
1,5-pentane diol	242	51.9	7
2,3-butane diol	182	51.8	8
1,2-propane diol	188	54.1	9

As evident from PXRD analysis the use of these solvents under given solvothermal reaction conditions (215 °C, 24 h) led to very different compounds and crystalline structures (see Figure 2). While the solvothermal reaction in monoethylene glycol (1), glycerol (2) and diethylene glycol (3) did not lead to any  $\text{Li}_2\text{CoPO}_4\text{F}$  formation, the use of tetraethylene glycol (4) gave  $\text{Li}_2\text{CoPO}_4\text{F}$  as secondary phase, besides  $\text{Li}_3\text{PO}_4$ ,  $\text{LiCoPO}_4^{\text{tetra}}$  and  $\text{LiF}$ .<sup>38</sup> Structurally comparable but with a

lower solvent polarity, tetraethylene glycol dimethyl ether (5) resulted in only very small amounts of  $\text{Li}_2\text{CoPO}_4\text{F}$ , with a larger portion of  $\text{Li}_3\text{PO}_4$ ,  $\text{LiCoPO}_4^{\text{tetra}}$  and  $\text{LiF}$ . The reason for this is most probably the difference in polarity compared to tetraethylene glycol.

Using PEG-400 (6), with a longer ethylene glycol chain, similar results as for solvent (5) were obtained. Consequently we have tested 1,5-pentane diol (7), which is comparable to tetraethylene glycol (4) in polarity and structurally closely related to diethylene glycol (3). The powder X-ray diffraction pattern of the product from 1,5-pentane diol (7) shows almost phase pure  $\text{Li}_2\text{CoPO}_4\text{F}$  with  $\text{CoHPO}_4 \cdot \text{H}_2\text{O}$  as secondary phase. Therefore, 2,3-butane diol (8) and 1,2-propane diol (9) were applied in addition to investigate the influence of the solvent polarity in more detail.

While the products synthesized using 2,3-butane diol are the same as those obtained using 1,5-pentane diol (7), phase pure  $\text{Li}_2\text{CoPO}_4\text{F}$  could be synthesized from 1,2-propane diol (9) again indicating that the solvent polarity plays an important role.

An additional parameter that needs to be considered in these reactions is the boiling point of the solvent. When using 2,3-butane diol (bp = 182 °C) or 1,2-propane diol (bp = 188 °C) the boiling point is below the reaction temperature of 215 °C, thus resulting in an increase of the pressure up to 20 bar in the autoclave during the synthesis. However, 1,5-pentane diol (7) has a boiling point of 242 °C, but a pressure of 22 bar at the end of the reaction was observed. In this case, a side reaction of the solvent can be considered, which was further investigated via <sup>1</sup>H- and <sup>13</sup>C-NMR studies. We could observe a ring closing reaction from 1,5-pentane diol to tetrahydropyran that explains the increase of the pressure during the synthesis, since the boiling point of tetrahydropyran is 88 °C. This observation is related to the described phosphate-based catalyzed ring closing reactions of 1,*n*-diols.<sup>39</sup> An analogous ring closing reaction of diethylene glycol (3) to 1,4-dioxane (bp 101 °C) was not observed.

According to these investigations two parameters seem to be very important for a successful synthesis of phase pure  $\text{Li}_2\text{CoPO}_4\text{F}$ . First, the solvent polarity  $E_T(30)$  needs to be adjusted in a rather narrow range between 51.8 and 54.1 kcal  $\text{mol}^{-1}$ . This can be seen by comparing the products synthesized from solvents 1–3 and 4–6. Since no pressure is built-up during these syntheses, the solubility of the used chemicals in the applied solvent and the formation of the products, especially  $\text{Li}_2\text{CoPO}_4\text{F}$ , during the synthesis depends only on the used reaction solvent. Second, autogenous pressure is apparently also necessary to obtain  $\text{Li}_2\text{CoPO}_4\text{F}$  as main phase from this solvothermal synthesis. During the synthesis using solvent 7–9 autogenous pressure (20 bar) was detected and  $\text{Li}_2\text{CoPO}_4\text{F}$  forms as main phase. As an additional synthesis variable the reaction time was investigated. After 24 h almost phase pure  $\text{Li}_2\text{CoPO}_4\text{F}$  has been formed when 1,5-pentane diol or/and 2,3-butane diol were used (1,2-propane diol led to a phase pure product). The powder X-ray diffraction patterns of products obtained from the solvents (7–9) and an increased reaction time of 36 h are shown in Figure S1. In some cases small amounts of  $\text{LiCoPO}_4$  as secondary phase (see Figure S5) were found. The exact growth mechanism of  $\text{Li}_2\text{CoPO}_4\text{F}$  from solvents 7–9 is under investigation, but is not topic of this publication.

The scanning electron microscopy (SEM) images of the reaction products ( $\text{Li}_2\text{CoPO}_4\text{F}$ ) using 1,5-pentane diol, 2,3-

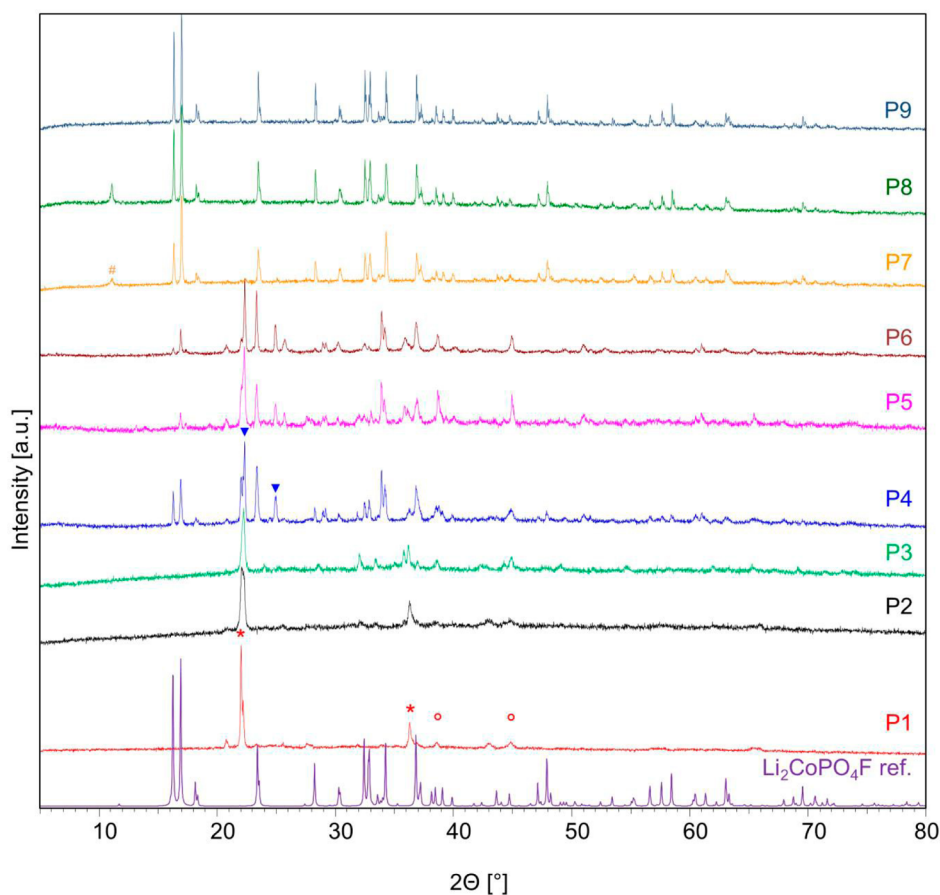


**Figure 2.** PXRD of the products (P1–P9) from different solvents (1–9) after solvothermal synthesis (215 °C, 24 h); Reference plot ( $\text{Li}_2\text{CoPO}_4\text{F}$  ref from ref 11) of  $\text{Li}_2\text{CoPO}_4\text{F}$  at the bottom. Strongest reflexes of secondary phases are marked at first occurrence: asterisk (\*) labels  $\text{LiCoPO}_4^{\text{tetra}}$ , cycle (deg) labels  $\text{LiF}$ , triangle (▼) labels  $\text{Li}_3\text{PO}_4$  and hashtag (#) labels  $\text{CoHPO}_4\cdot\text{H}_2\text{O}$ .

butane diol and 1,2-propane diol are shown in Figure 3. Crystalline particles with plank-like morphology were obtained from 1,5-pentane diol (Figure 3a), with an average length of 14  $\mu\text{m}$ , a width and height of 4 and 1  $\mu\text{m}$ , respectively. The reactions in 2,3-butane diol and 1,2-propane diol resulted in significantly smaller particles. Although the molecular structures of the two solvents are comparable, different product morphologies were obtained. 2,3-butane diol led to square platelets (Figure 3b) with edges of an average length of 2  $\mu\text{m}$  and a thickness of 300 nm. Rod-like morphologies with a square cross section (Figure 3c) were obtained for the products of the reactions using 1,2-propane diol. These rods have a maximum length of 3  $\mu\text{m}$  with a height and width of about 500 nm. While transmission electron microscopy (TEM) images could be taken for  $\text{Li}_2\text{CoPO}_4\text{F}$  particles synthesized from 1,5-pentane diol and 2,3-butane diol (see Figure S2), particles synthesized from 1,2-propane diol degenerated during TEM analysis, hence did not allow to obtain an accurate diffraction pattern to investigate the crystal growth of the  $\text{Li}_2\text{CoPO}_4\text{F}$  particles. For both crystalline compounds synthesized from 1,5-pentane diol and 2,3-butane diol a preferred crystal growth orientation was found. Crystals from 1,5-pentane diol show a preferred orientation resulting in a large (200)-plane, where the long edge of around 14  $\mu\text{m}$  is parallel to the  $b$ -axes (Figure S2a). For the square platelets synthesized from 2,3-butane diol a preferred orientation, in which the square plane belongs to the (002)-plane of the crystal (Figure S2b) is observed. These investigations are in good agreement with the observed

preferred orientations from Rietveld refinement (see Figure S5). For particles synthesized from solvent 1,5-pentane diol a more pronounced (200) reflection was detected, while for particles from solvent 2,3-butane diol a slightly stronger (002) reflection was observed. In agreement with electron microscopy images,  $\text{N}_2$ -sorption measurements show specific surface areas of 1.4  $\text{m}^2 \text{g}^{-1}$ , 3.9  $\text{m}^2 \text{g}^{-1}$ , and 1.5  $\text{m}^2 \text{g}^{-1}$  for the products synthesized from solvent 7, 8 and 9, respectively, clearly indicating the large crystallite size.

**Electrochemical Testing.** The three compounds (Mx) synthesized from 1,5-pentane diol (M7), 2,3-butane diol (M8) and 1,2-propane diol (M9) (reaction conditions: 215 °C, 36 h) were chosen as candidates for electrochemical investigations. To this end, the particles were prepared with vapor grown carbon fibers via a ball milling procedure and additional annealing at either 500 or 600 °C according to our previous work.<sup>28</sup> Since we obtained  $\text{Co}_2\text{P}$  impurities after the annealing step at 700 °C,<sup>28</sup> we decided to use lower annealing temperatures, to avoid any phase impurities. Prior to the electrochemical testing, the influence of the carbon coating procedure on the phase purity was investigated by *ex-situ* PXRD measurements (Figure S3). As can be seen no new phases originated in the annealing step. However, for M7 the intensity of the reflection at  $2\theta$  36° ( $\text{LiCoPO}_4$ ) increases with higher annealing temperatures. For M8 a broad reflection at  $2\theta$  26.4° appears after carbon coating that can be assigned to the nonmilled vapor grown carbon fibers. These fibers are also seen in the SEM images (Figure S4e,f). In addition, the reflection for

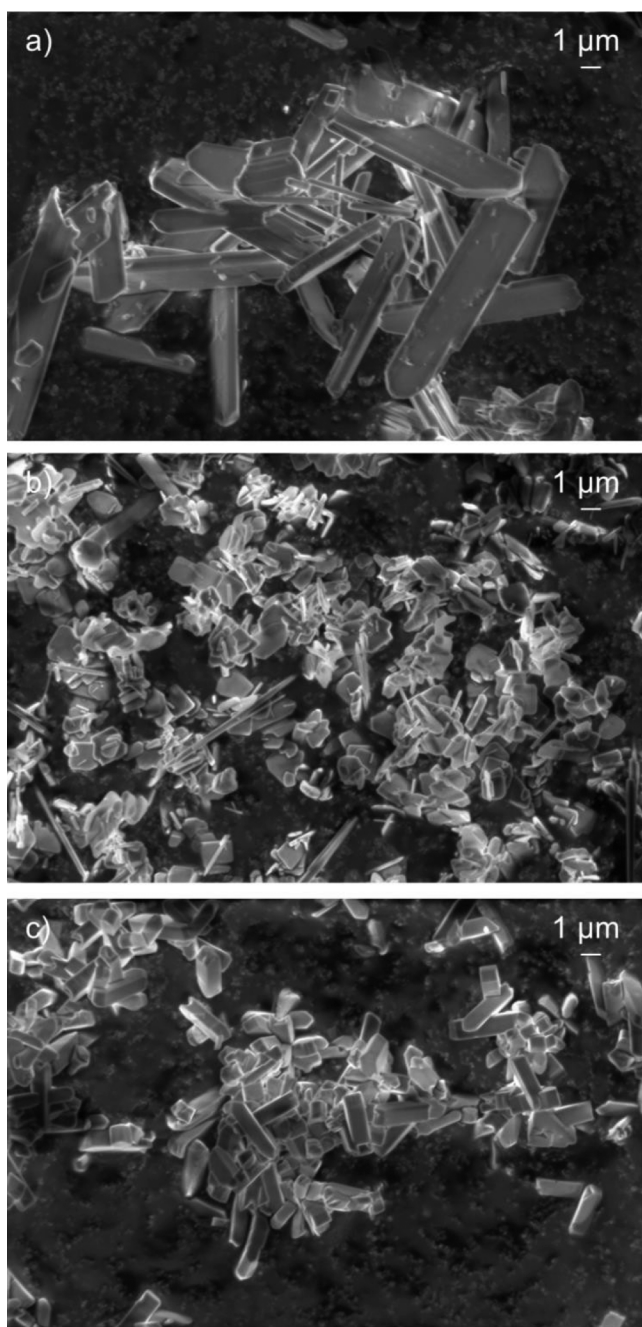


**Figure 3.** SEM images of  $\text{Li}_2\text{CoPO}_4\text{F}$  particles from different solvents after 36 h reaction time (a) M7, (b) M8, and (c) M9. The scale bar corresponds to 1  $\mu\text{m}$ .

the impurity phase  $\text{LiCoPO}_4$  became more pronounced. This is in agreement with the results from Rietveld refinement (see Figure S5, Table S1). The SEM images show for all samples M7, M8, and M9 a strong influence of the milling process on the particle morphology.

Submicron particles with no specific morphologies were obtained after the carbon coating procedure for all compounds. Results of the BET analysis from  $\text{N}_2$ -sorption measurements and the amount of carbon in the samples are summarized in Table 2. The amount of carbon in all samples ranges from 14–15 wt %. While the carbon coating procedure for M7 and M9 leads to specific surface areas (SSA) between 50 and 60  $\text{m}^2 \text{g}^{-1}$ , SSA of only around 25  $\text{m}^2 \text{g}^{-1}$  were obtained for M8. As a

**Table 2.** Specific Surface Areas and Carbon Content of  $\text{Li}_2\text{CoPO}_4\text{F}$  Particles Prepared for Electrochemical Testing

compound [abbreviation]	specific surface area [ $\text{m}^2 \text{g}^{-1}$ ]	carbon content [wt %]
7_500	51	14.1
7_600	58	13.9
8_500	22	15.1
8_600	27	15.1
9_500	52	14
9_600	56	13.9

general trend, slightly higher specific surface areas are obtained with higher annealing temperatures.

To obtain a better overview on the preparation of the  $\text{Li}_2\text{CoPO}_4\text{F}$  containing electrodes, the electrochemical testing protocols were similar to our previously described work.<sup>28</sup> Discharge capacities/voltage curves for the first five cycles (constant charge and discharge rates of 0.1 C for the first three cycles) of half-cells prepared from carbon coated particles after different annealing temperatures are shown in Figure 4. All six samples show initial discharge capacities of 143  $\text{mAh g}^{-1}$ , which is the theoretical capacity of  $\text{Li}_2\text{CoPO}_4\text{F}$  upon extraction of one stoichiometric equivalent of one lithium per formula unit. These results are in very good agreement with previous reports for samples synthesized via solid state reactions.<sup>12,14,40</sup> Furthermore, the initial discharge capacities obtained for the first five cycles are higher than the previously reported ones.<sup>28</sup> These very high initial discharge capacities can be attributed to very small (nano sized) carbon coated  $\text{Li}_2\text{CoPO}_4\text{F}$  particles similar to carbon coated  $\text{LiMPO}_4$  ( $M = \text{Fe}, \text{Mn}, \text{Co}$ ) materials.<sup>41–43</sup>

For the fourth and fifth cycle the discharge rate was increased to 1.0 C. An influence of the annealing temperature on the discharge capacities for these two cycles of the differently prepared compounds is obvious. Samples prepared with an annealing temperature of 500  $^\circ\text{C}$  show a stronger decrease of the discharge capacities (as compared to those of products annealed at 600  $^\circ\text{C}$ ). M7\_500 shows a drop in the discharge capacity from 135  $\text{mAh g}^{-1}$  (third cycle) to 83  $\text{mAh g}^{-1}$  (61% retention) for the fourth cycle. This effect is significantly reduced with a higher annealing temperature (600  $^\circ\text{C}$ ). The capacity loss shows a retention of 85%, from 131  $\text{mAh g}^{-1}$  to 112  $\text{mAh g}^{-1}$ .

Furthermore, increasing the annealing temperature after carbon coating eliminates the continuous capacity loss to a large extent (see Figure 4). For carbon coated particles annealed at 600  $^\circ\text{C}$  only little discharge capacity losses could be observed when the discharge rate was increased from 0.1 to 1.0 C (from 141  $\text{mAh g}^{-1}$  for the third cycle to 133  $\text{mAh g}^{-1}$  for the fourth cycle, 94% retention).

## CONCLUSIONS

In this paper we have presented for the first time a one-pot solution-based route toward  $\text{Li}_2\text{CoPO}_4\text{F}$ . The macroscopic morphology of the phase pure, crystalline  $\text{Li}_2\text{CoPO}_4\text{F}$  can be deliberately adjusted by careful selection of the organic reaction medium for solvothermal processing. The dependence of the preferred crystal growth orientation of the  $\text{Li}_2\text{CoPO}_4\text{F}$  particles on the used organic solvent was proven. Carbon coating of the solvothermally prepared  $\text{Li}_2\text{CoPO}_4\text{F}$  particles resulted in visible morphological changes of the  $\text{Li}_2\text{CoPO}_4\text{F}$  particles.

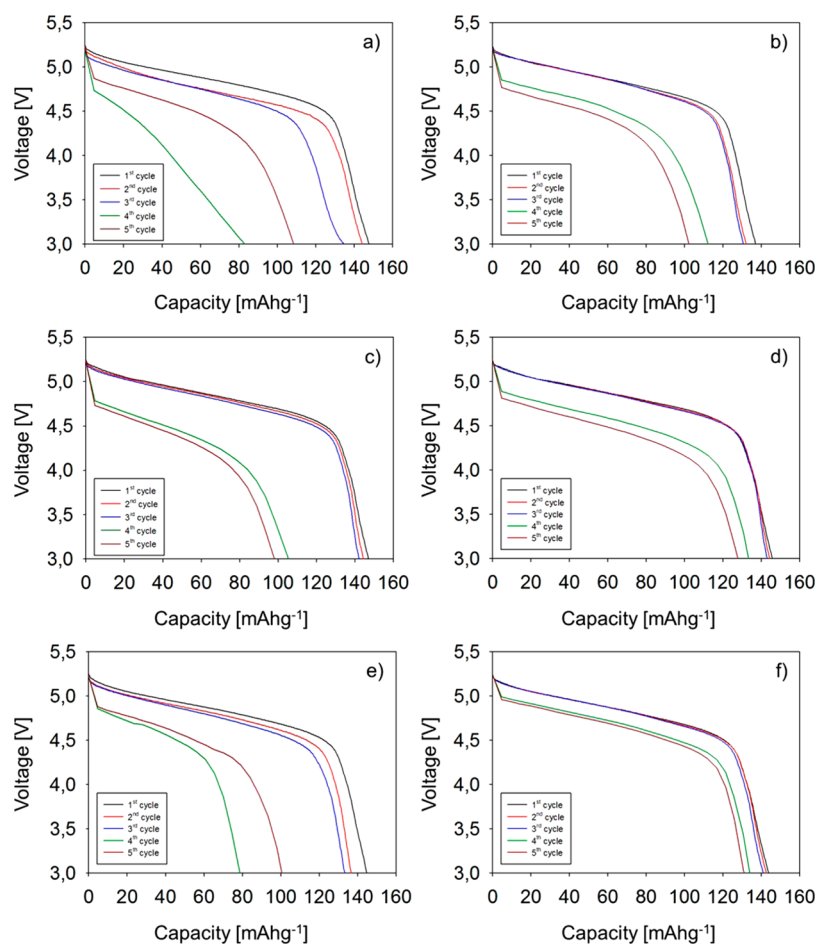


**Figure 4.** First five discharge capacities at various C-rates (first three cycles at 0.1 C; fourth and fifth cycle 1.0 C) after constant charging at 0.1 C from different carbon coated particles; (a) and (b) M7\_500 and M7\_600, respectively; (c) and (d) M8\_500 and M8\_600, respectively; (e) and (f) M9\_500 and M9\_600, respectively.

The electrochemical performance of the carbon coated compounds was tested in half cells against lithium for samples prepared with different annealing temperatures in the carbon coating process. A significant influence of the synthetic procedure on the electrochemical performance, dependent on the different annealing temperatures, was observed.

For low charge and discharge rates (0.1 C) almost all samples showed a capacity of  $143 \text{ mAh g}^{-1}$  corresponding to the theoretical capacity for the extraction of one lithium ion per formula unit. Capacity loss is observed at higher discharge rates (1.0 C), probably due to minor decomposition reactions and low diffusion kinetics in the half-cells, but further investigations on this topic are still needed.

## ■ ASSOCIATED CONTENT

### 📄 Supporting Information

The Supporting Information is available free of charge on the ACS Publications website at DOI: [10.1021/acs.cgd.6b00573](https://doi.org/10.1021/acs.cgd.6b00573).

PXRD patterns of  $\text{Li}_2\text{CoPO}_4\text{F}$  compounds synthesized with a reaction time of 36 h are shown in Figure S1. Figure S2 shows the TEM images of  $\text{Li}_2\text{CoPO}_4\text{F}$  particles including electron diffraction patterns. The PXRD pattern of carbon coated  $\text{Li}_2\text{CoPO}_4\text{F}$  materials are shown in Figure S3, while Figure S4 shows SEM images of these compounds. Rietveld refinements of as-synthesized and carbon coated compounds are seen in

Figure S5, refined unit cell parameters and compound contents are summarized in Table S1 (PDF)

## ■ AUTHOR INFORMATION

### Corresponding Authors

\*(J.S.) E-mail: [juergen.schoiber@sbg.ac.at](mailto:juergen.schoiber@sbg.ac.at).

\*(N.H.) E-mail: [nicola.huesing@sbg.ac.at](mailto:nicola.huesing@sbg.ac.at).

### Notes

The authors declare no competing financial interest.

## ■ ACKNOWLEDGMENTS

This work was financially supported by Toyota Motor Europe NV/SA. We thank G. Tippelt for the PXRD, G. J. Redhammer for scientific discussions, and M. Suljic for the  $\text{N}_2$ -sorption measurements (University of Salzburg) as well as M. Lang for elemental analysis (University of Ulm).

## ■ REFERENCES

- (1) Okada, S.; Ueno, M.; Uebou, Y.; Yamaki, J. *J. Power Sources* **2005**, *146*, 565–569.
- (2) Ramesh, T. N.; Lee, K. T.; Ellis, B. L.; Nazar, L. F. *Electrochem. Solid-State Lett.* **2010**, *13*, A43–A47.
- (3) Kim, S. W.; Seo, D. H.; Kim, H.; Park, K. Y.; Kang, K. *Phys. Chem. Chem. Phys.* **2012**, *14*, 3299–3303.
- (4) Recham, N.; Chotard, J. N.; Jumas, J. C.; Laffont, L.; Armand, M.; Tarascon, J. M. *Chem. Mater.* **2010**, *22*, 1142–1148.

- (5) Barker, J.; Saidi, M. Y.; Swoyer, J. L. *J. Electrochem. Soc.* **2003**, *150*, A1394–A1398.
- (6) Kubota, K.; Yokoh, K.; Yabuuchi, N.; Komaba, S. *Electrochemistry* **2014**, *82*, 909–911.
- (7) Ellis, B. L.; Makahnouk, W. R. M.; Makimura, Y.; Toghill, K.; Nazar, L. F. *Nat. Mater.* **2007**, *6*, 749–753.
- (8) Zhao, J.; He, J.; Ding, X.; Zhou, J.; Ma, Y.; Wu, S.; Huang, R. J. *J. Power Sources* **2010**, *195*, 6854–6859.
- (9) Yu, J.; Rosso, K. M.; Zhang, J. G.; Liu, J. *J. Mater. Chem.* **2011**, *21*, 12054–12058.
- (10) Khasanova, N. R.; Drozhzhin, O. A.; Storozhilova, D. A.; Delmas, C.; Antipov, E. V. *Chem. Mater.* **2012**, *24*, 4271–4273.
- (11) Hadermann, J.; Abakumov, A. M.; Turner, S.; Hafideddine, Z.; Khasanova, N. R.; Antipov, E. V.; Van Tendeloo, G. *Chem. Mater.* **2011**, *23*, 3540–3545.
- (12) Wu, X.; Wang, S.; Lin, X.; Zhong, G.; Gong, Z.; Yang, Y. *J. Mater. Chem. A* **2014**, *2*, 1006–1013.
- (13) Lee, S.; Park, S. S. *J. Solid State Chem.* **2013**, *204*, 329–334.
- (14) Okumura, T.; Shikano, M.; Yamaguchi, Y.; Kobayashi, H. *Chem. Mater.* **2015**, *27*, 2839–2847.
- (15) Wu, X.; Gong, Z.; Tan, S.; Yang, Y. *J. Power Sources* **2012**, *220*, 122–129.
- (16) Amaresh, S.; Kim, G. J.; Karthikeyan, K.; Aravindan, V.; Chung, K. Y.; Cho, B. W.; Lee, Y. S. *Phys. Chem. Chem. Phys.* **2012**, *14*, 11904–11909.
- (17) Khasanova, N. R.; Drozhzhin, O. A.; Fedotov, S. S.; Storozhilova, D. A.; Panin, R. V.; Antipov, E. V. *Beilstein J. Nanotechnol.* **2013**, *4*, 860–867.
- (18) Amaresh, S.; Karthikeyan, K.; Kim, K. J.; Kim, M. C.; Chung, K. Y.; Cho, B. W.; Lee, Y. S. *J. Power Sources* **2013**, *244*, 395–402.
- (19) Markevich, E.; Salitra, G.; Fridman, K.; Sharabi, R.; Gershinsky, G.; Garsuch, A.; Semrau, G.; Schmidt, M. A.; Aurbach, D. *Langmuir* **2014**, *30*, 7414–7424.
- (20) Ortiz, G. F.; López, M. C.; Li, Y.; McDonald, M. J.; Cabello, M.; Tirado, J. L.; Yang, Y. *Sci. Rep.* **2016**, *6*, No. 20656.
- (21) Khasanova, N. R.; Gavrilov, A. N.; Antipov, E. V.; Bramnik, K. G.; Hibst, H. *J. Power Sources* **2011**, *196*, 355–360.
- (22) Kosova, N. V.; Devyatkina, E. T.; Slobodyuk, A. B. *Solid State Ionics* **2012**, *225*, 570–574.
- (23) Lin, X.; Hou, X.; Wu, X.; Wang, S.; Gao, M.; Yang, Y. *RSC Adv.* **2014**, *4*, 40985–40993.
- (24) Recham, N.; Chotard, J. N.; Dupont, L.; Djellab, K.; Armand, M.; Tarascon, J. M. *J. Electrochem. Soc.* **2009**, *156*, A993–A999.
- (25) Ellis, B. L.; Makahnouk, W. R. M.; Rowan-Weetaluktuk, W. N.; Ryan, D. H.; Nazar, L. F. *Chem. Mater.* **2010**, *22*, 1059–1070.
- (26) Ellis, B. L.; Ramesh, T. N.; Rowan-Weetaluktuk, W. N.; Ryan, D. H.; Nazar, L. F. *J. Mater. Chem.* **2012**, *22*, 4759–4766.
- (27) Yakubovich, O. V.; Karimova, O. V.; Mel'nikov, O. K. *Acta Crystallogr., Sect. C: Cryst. Struct. Commun.* **1997**, *53*, 395–397.
- (28) Schoiber, J.; Berger, R. F. J.; Yada, C.; Miki, H.; Hüsing, N. *J. Electrochem. Soc.* **2015**, *162*, A2679–A2683.
- (29) Rodriguez-Carvajal, J. *Phys. B* **1993**, *192*, 55–69.
- (30) Jensen, K. M. Ø.; Christensen, M.; Gunnlaugsson, H. P.; Lock, N.; Bøjesen, E. D.; Proffen, T.; Iversen, B. B. *Chem. Mater.* **2013**, *25*, 2282–2290.
- (31) Brunauer, S.; Emmett, P. H.; Teller, E. *J. Am. Chem. Soc.* **1938**, *60*, 309–319.
- (32) Yang, H.; Wu, X. L.; Cao, M. H.; Guo, Y. G. *J. Phys. Chem. C* **2009**, *113*, 3345–3351.
- (33) Tripathi, R.; Ramesh, T. N.; Ellis, B. L.; Nazar, L. F. *Angew. Chem., Int. Ed.* **2010**, *49*, 8738–8742.
- (34) Kuezma, M.; Devaraj, S.; Balaya, P. *J. Mater. Chem.* **2012**, *22*, 21279–21284.
- (35) Guo, H.; Wu, C.; Xie, J.; Zhang, S.; Cao, G.; Zhao, X. *J. Mater. Chem. A* **2014**, *2*, 10581–10588.
- (36) Brutti, S.; Manzi, J.; De Bonis, A.; Di Lecce, D.; Vitucci, F.; Paolone, A.; Trequattrini, F.; Panero, S. *Mater. Lett.* **2015**, *145*, 324–327.
- (37) Reichardt, C. *Chem. Rev.* **1994**, *94*, 2319–2358.
- (38) Jähne, C.; Neef, C.; Koo, C.; Meyer, H.; Klingeler, R. *J. Mater. Chem. A* **2013**, *1*, 2856–2862.
- (39) Patel, S. M.; Chudasama, U. V.; Ganeshpure, P. A. *Green Chem.* **2001**, *3*, 143–145.
- (40) Wang, D.; Xiao, J.; Xu, W.; Nie, Z.; Wang, C.; Graff, G.; Zhang, J. *J. Power Sources* **2011**, *196*, 2241–2245.
- (41) Bramnik, N. N.; Bramnik, K. G.; Baetz, C.; Ehrenberg, H. *J. Power Sources* **2005**, *145*, 74–81.
- (42) Liu, H.; Zhang, H. P.; Fu, L. J.; Wu, Y. P.; Wu, H. Q.; Li, C. J. *J. Power Sources* **2006**, *159*, 717–720.
- (43) Lee, K. T.; Cho, J. *Nano Today* **2011**, *6*, 28–41.